Available online at www.sciencedirect.com
ScienceDirect
Journal of Computational Physics 227 (2008) 2845–2863
JOURNAL OF COMPUTATIONAL PHYSICS
www.elsevier.com/locate/jcp

Heuristic *a posteriori* estimation of error due to dissipation in finite volume schemes and application to mesh adaptation

Richard P. Dwight *

German Aerospace Center (DLR), Lilienthalplatz, 7, Braunschweig D-38108, Germany

Received 25 July 2007; received in revised form 24 October 2007; accepted 15 November 2007
Available online 24 November 2007

Abstract

A heuristic method is proposed to estimate *a posteriori* that part of the total discretization error which is attributable to the smoothing effect of added dissipation, for finite volume discretizations of the Euler equations. This is achieved by observing variation in a functional of the solution as the level of dissipation is varied, and it is deduced for certain test-cases that the dissipation alone accounts for the majority of the functional error. Based on this result an error estimator and mesh adaptation indicator is proposed for functionals, relying on the solution of an adjoint problem. The scheme is considerably implementationally simpler and computationally cheaper than other recently proposed *a posteriori* error estimators for finite volume schemes, but does not account for all sources of error. In mind of this, emphasis is placed on numerical evaluation of the performance of the indicator, and it is shown to be extremely effective in both estimating and reducing error for a range of 2d and 3d flows.

Keywords: *A posteriori* error estimation; Goal-oriented mesh adaptation; Finite volume methods; Dissipation error; Adjoint problem

1. Introduction

One of the principal advantages of unstructured mesh methods is the readiness with which the mesh can be locally refined to suit the solution. The expectation is that by concentrating points in regions of interest, important flow field features, such as shocks and vortices, can be resolved accurately with significantly less points than required for a globally finer mesh. However, it is not necessarily the case that adding points locally will reduce global measures of error. An example of this phenomenon was given by Warren et al. [1], who examined a high-transonic NACA0012 case with a fish-tail shock structure, where the position of the normal shock in the fish-tail was of interest. Repeatedly local refining the grid using an indicator based on local gradients of pressure, produced a sequence of estimates for the shock position which converged to value different from that obtained by globally refining the mesh. Nor is this an isolated example, here a similar result is given for an unremarkable transonic aerofoil.

* Tel.: +49 531 295 2893; fax: +49 531 295 2320.
E-mail address: richard.dwight@dlr.de

0021-9991/$ - see front matter © 2007 Elsevier Inc. All rights reserved.
doi:10.1016/j.jcp.2007.11.020

The cause of this effect is simply that the shock position and strength are dependant on the flow elsewhere in the field. Errors produced in the discretization upstream of the shock, in smooth regions of the flow, are convected to the shock and modify it. The regions that produce these errors are not adapted because the solution is locally smooth, and hence these discretization errors are not reduced. In short: for hyperbolic problems mesh adaptation is a global problem, and feature-based schemes are almost always local.

In response to this situation an extremely successful theory of *a posteriori* error estimation and mesh adaptation has been developed in the context of finite element methods [2–8]. Using the adjoint (or dual) problem to the problem of interest, which serves to relate local errors in the field to the error in a specified functional of interest J, it is possible to derive exact *error representation formulas* which have no dependence on the exact solution of the original problem [9,10]. In practice the functional may be taken to be an engineering quantity of interest, such as lift or drag. While this theory relies on the Galerkin orthogonality of the finite element schemes used, currently the dominant methods in use for aerodynamic applications are second-order finite volume codes, an example of which is applied in this work, the DLR *TAU*-Code [11,12]. An alternative but related approach to the same problem which is not considered here is *adaptive multiresolution analysis*, wherein a hierarchy of discretizations are examined in order to identify the level of solution resolution required locally [13–16].

One approach to obtain error representation formulas for finite volume schemes is due to Venditti and Darmofal [17] and Pierce and Giles [18] and recently applied to sonic boom prediction by Jones et al. [19], uses a globally refined grid to obtain an estimate of the local residual error, which is then related to the functional error via the adjoint solution. While the method gives an accurate error estimator, there are substantial difficulties associated with the implementation of such schemes. In particular second-order interpolation of discontinuous solutions from coarse grids onto fine grids is needed. Also efficient evaluation of the fine grid residual without explicit construction and storage of this grid is difficult; explicit storage would represent a memory bottleneck. These problems come in addition to the problematic issue of robust and efficient solution of the adjoint equations for viscous flows in complex geometries, which has only recently become tractable [20–23]. The only application of these techniques to truly complex geometries to date is due to Nemec and Aftosmis [24] who used a Cartesian mesh method which allows cheap explicit construction of and interpolation onto globally refined grids.

In light of these difficulties an alternative approach was proposed in [25] and is developed further here, which still requires an adjoint solution, but which is considerably simpler implementationally, as well as being cheaper to evaluate. We consider the sensitivity of the functional of interest to the level of dissipation introduced by the numerical flux. The particular flux examined is the artificial viscosity scheme due to Jameson et al. [26], with two parameters $k^{(2)}$ and $k^{(4)}$ which control respectively the levels of explicitly added second- and fourth-derivative dissipation. Since the dissipation scales as a power of the mesh spacing h, grid converged solutions are independent of the dissipation parameters. For finite grids any extant sensitivity corresponds to numerical errors introduced by the dissipation, and it will be seen how a quantitative error estimate may be constructed from this information.

In order to illustrate the approach, but without going into detail or providing justification here (which will be given in Section 4), we present a schematic of the model of error we use in Fig. 1. Broadly, as the level of dissipation is increased the solution is smoothed increasing the error; as the level of dissipation is reduced instabilities arise in the solution, usually in the form of high-frequency oscillations, and eventually the scheme becomes unstable. A desirable and typically used level of dissipation is indicated by the circle, and it our intention to extrapolate from here onto the zero dissipation limit, thereby approximately eliminating that component of error in the solution due to the dissipation.

Further, by regarding $k^{(2)}$ and $k^{(4)}$ as quantities defined independently at each mesh point, a local measure of goal function sensitivity is also obtained, which serves as an indicator for mesh refinement. The sensitivities themselves may be easily and accurately evaluated using an adjoint method, and no interpolation or fine grids are necessary.

An obvious deficit of this approach is that sources of error other than those due to the dissipation are invisible to the sensor. Therefore, a procedure is developed to numerically estimate *a posteriori* the proportion of dissipation error to total discretization error in a functional. In application to 2d and 3d test cases at a variety

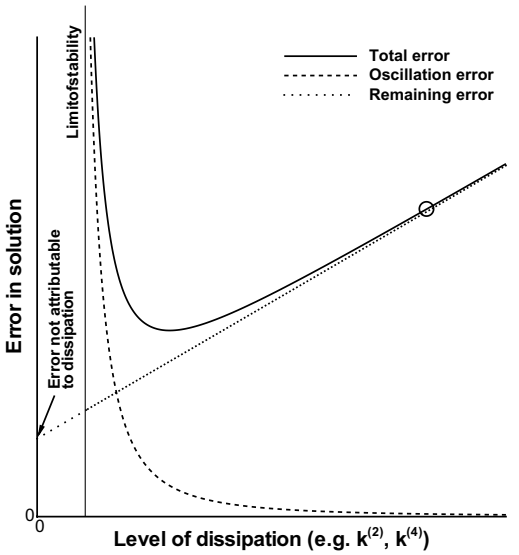

Fig. 1. Schematic of error in solution against level of dissipation.

of mesh resolutions, always more than 90% of the error in drag is found to be attributable to the smoothing influence of dissipation.

The performance of the error estimator and indicator in lift and drag, for sub-, trans- and supersonic test-cases in 2d and 3d is examined. In each case the true error in the functional (measured against reference solutions obtained on uniformly refined grids) is plotted against the number of nodes in the mesh. Feature-based and global adaptation results are also given for comparison. It is seen in all cases that significantly greater functional accuracy is achieved with fewer mesh points for error indicator adapted grids, and that the estimated error consistently agrees well with the true error.

2. Discretization of the governing equations

Consider the stationary Euler equations for a compressible fluid in conservative variables $w = (\rho, \rho u, \rho v, \rho E)$, with analytic flux f, on the domain Ω:

$$\nabla \cdot f = 0 \quad \text{on } \Omega, \text{ where } f = \begin{bmatrix} \rho u & \rho v \\ \rho u^2 + p & \rho uv \\ \rho uv & \rho v^2 + p \\ \rho uH & \rho vH \end{bmatrix}, \tag{1}$$

subject to slip boundary conditions on Γ the boundary of Ω. Here ρ, u, v, p, E and H are the fluid density, Cartesian velocity components, pressure, total energy and enthalpy respectively. This equation is discretized with the finite volume method on an unstructured grid with control volumes Ω_i with inner boundaries Γ_i:

$$\int_{\Omega_i} \nabla \cdot f \, \mathrm{d}\Omega \simeq \int_{\Gamma_i} \hat{f} \cdot n \, \mathrm{d}\Gamma + \int_{\Gamma_b} \hat{f}_b \cdot n \, \mathrm{d}\Gamma = 0, \quad \text{or} \quad R(w) = 0,$$

where $\hat{f}$ and $\hat{f}_b$ are numerical internal and boundary fluxes accounting for discontinuities at control volume interfaces, and R is the residual. It is well known that $\hat{f}$ must contain some added dissipation if the discretization is to be stable and capable of capturing shocks, see Section 3.

The flux chosen here is the popular artificial viscosity scheme due to Jameson, Schmidt and Turkel commonly called the JST scheme [26], which includes two user-specified parameters that control the level of dissipation. The flux across a grid face $\{ij\}$ with normal vector n_{ij} is written

$$\hat{f}_{ij}(w_i, w_j) = \frac{1}{2}\big(f(w_i) + f(w_j)\big)\cdot n_{ij} - \frac{1}{2}|\lambda_{ij}|\Big[\varepsilon^{(2)}_{ij}\{w_j - w_i\} - \varepsilon^{(4)}_{ij}\{L_j(w) - L_i(w)\}\Big], \tag{2}$$

where $|\lambda_{ij}|$ is the maximum convective eigenvalue at the face, and

$$L_i(w) = \sum_{j\in\mathcal{N}(i)} (w_j - w_i),$$

where $\mathcal{N}(i)$ is the set of neighbours of i, is an undivided unstructured grid discretization of a second-derivative ($\mathcal{O}(h^2)$, where h is the characteristic mesh spacing), so that (2) takes the form of a central difference of the exact flux, plus a second- and a fourth-derivative dissipation term. The coefficients $\varepsilon^{(2)}$ and $\varepsilon^{(4)}$ control the relative levels of these two dissipation terms

$$\varepsilon^{(2)}_{ij} = k^{(2)}\max(\Psi_i, \Psi_j)\Phi^{(2)}, \quad \varepsilon^{(4)}_{ij} = \max(k^{(4)} - \varepsilon^{(2)}_{ij}, 0)\Phi^{(4)}, \tag{3}$$

based on the shock switch

$$\Psi_i = \frac{\sum_{j\in\mathcal{N}(i)}|p_j - p_i|}{\sum_{j\in\mathcal{N}(i)}(p_j + p_i)}. \tag{4}$$

Some empirically derived corrections for mesh irregularity are contained in $\Phi^{(2)}$ and $\Phi^{(4)}$. The user-defined constants $k^{(2)}$ and $k^{(4)}$ take the default values of 1/2 and 1/64, respectively, and control the absolute levels of the two types of dissipation. The use of $k^{(4)} = 1/32$ is common for complex geometries and poor quality grids in order to improve stability.

The shock switch Ψ is designed to be $\mathcal{O}(1)$ near regions of large pressure gradient and $\mathcal{O}(h^2)$ elsewhere. Hence near a shock $\varepsilon^{(2)} \sim \mathcal{O}(1)$ and $\varepsilon^{(4)} = 0$, so that the scheme does not attempt to construct a fourth-derivative using a stencil which crosses a discontinuity. In smooth regions $\varepsilon^{(2)} \sim \mathcal{O}(h^2)$ and $\varepsilon^{(4)} \sim \mathcal{O}(1)$, so that both second- and fourth-differences are active and of $\mathcal{O}(h^3)$. Away from shocks the scheme is therefore second-order accurate in h as a result of the central difference in (2).

Finally, due to the cell-vertex metric, which results in mesh points lying on the boundary, the boundary condition may most easily be weakly formulated by setting $\hat{f}_b$ to the analytic flux over the boundary with zero normal velocity.

3. Review of dissipation in numerical methods

Almost all numerical methods for hyperbolic conservation laws rely on the deliberate addition of dissipation terms for two distinct purposes: numerical stabilization and discontinuity capturing.

There are a wide variety of ways in which dissipation may be introduced; *artificial viscosity schemes* (such as JST and generalizations using matrix coefficients [27]) explicitly add approximations of second- and higher-order derivative terms to the discretization [26]. Another possibility is *upwind schemes*, which use physically motivated weighting of the discretization stencil but may always be rewritten as a central difference plus a dissipation term [28–31]. More sophisticated methods such as *streamline-upwind* and *streamline-upwind Petrov–Galerkin* schemes take advantage of the fact that it is sufficient to add dissipation in the streamwise direction only [32], which is achieved by using modified the finite element test functions.

Regardless of their various origins these techniques may all be regarded as discretizations of a modified governing equation [31]. If the original conservation law is written

$$\nabla\cdot f(w) = 0, \tag{5}$$

then the continuous equation that is in fact discretized is typically

$$\nabla\cdot f(w_\epsilon) = \epsilon\nabla^2 w\big[+\epsilon_4\nabla^4 w + \cdots\big], \tag{6}$$

where the dissipation coefficient ϵ (and optionally ϵ_4, etc.) is defined by the particular scheme under consideration. At the very least ϵ should approach zero as the grid spacing h approaches zero, so that in the fine-mesh limit the influence of the dissipation disappears and the scheme has the potential to be a consistent discretization of (5). Clearly dissipation has a negative effect on accuracy, and an important aspect of the design of numerical schemes is the compromise between accuracy and stability.

Discontinuity capturing requires only that $\epsilon > 0$ in (6), given which (for smooth initial conditions) the solution w_ϵ is smooth for all time and

$$\lim_{\epsilon \to 0} w_\epsilon = w,$$

where w is here a vanishing viscosity solution of (5). This result together with numerical conservation gives the property of shock capturing.

The constraints placed by stability on the dissipation are more stringent. Linear stability results based on Fourier analysis place a non-zero lower bound on the amount of dissipation required for spurious solution oscillations to be damped. Non-linear analysis gives similar bounds based on reduction of total solution variation [31]. However, such results tend to have a limited validity and usefulness, for example in more than one dimension the Euler equations do not satisfy any variation diminishing property, and it is difficult to build total variation diminishing schemes of greater than first-order. As a result, in schemes typically used in practice (e.g. JST with default coefficients) some low level of spurious oscillation is almost always present (maybe only visible in entropy), and scheme design is in part a compromise between oscillation and dissipation.

So we may identify two competing modes of solution error that vary as the dissipation is reduced: error due to unphysical oscillations which increases, and "smearing" error due to the introduction of unphysical entropy, which decreases. A typical example of this trade-off is seen in Fig. 2 for a transonic NACA0012 aerofoil for the JST scheme with two strong shocks and various values of $k^{(2)}$ and $k^{(4)}$. Shown are surface pressure and entropy distributions, the latter is chosen for its high sensitivity to solution oscillations. In this inviscid flow entropy should be constant away from shocks, the extent to which it varies is therefore a measure of solution error. For the default dissipation level the shock is resolved within four mesh points, (as compared to the theoretical minimum of three mesh points, given no sub-cell resolution). As dissipation is reduced, sharpening of the shock, amplification of oscillations, and reduction of spurious entropy production near the nose are all clearly evident.

Finally note that higher dissipation levels often imply a problem which is easier (and cheaper) to solve. For example the case just presented was solved in about 300, 400 and 1000 multigrid cycles for high, default and low dissipation levels, respectively. This is of great significance, as the accuracy achieved for a given computation effort is of more practical interest than the accuracy achieved for a given number of mesh points.

4. Empirical estimation of error attributable to dissipation

In this section we attempt to quantify for some specific inviscid cases that part of the error in the flow solution which may be attributed to the smoothing effect of the explicitly added dissipation. In order to do so we attempt to isolate it from error due to spurious oscillations and error due to all other aspects of the spatial discretization, in so far as this is possible.

The latter is achieved by varying the level of added dissipation using the coefficients $k^{(2)}$ and $k^{(4)}$ and extrapolating onto the zero dissipation case. This is complicated by the stability limit below which the coefficients may not be decreased and the increase of oscillation error as dissipation is reduced. In order to milden the effect of this second problem we regard error in integrated force coefficients, which are less affected by the regular spurious oscillations than the solution itself.

The purpose of these calculations is two-fold: to demonstrate that the contribution of added dissipation error, (a) dominates other sources of discretization error in the force coefficients by a wide margin, and (b) varies approximately linearly with the dissipation coefficients in the range in which we are interested. Thus the well-known importance of dissipation to solution accuracy is quantified in an empirical manner.

4.1. A model for dissipation error

Consider an inviscid subsonic NACA0012 aerofoil at an angle of attack of 0° and an onflow Mach number of 0.5. Under these conditions the exact force coefficients are known and will be used as reference values in the

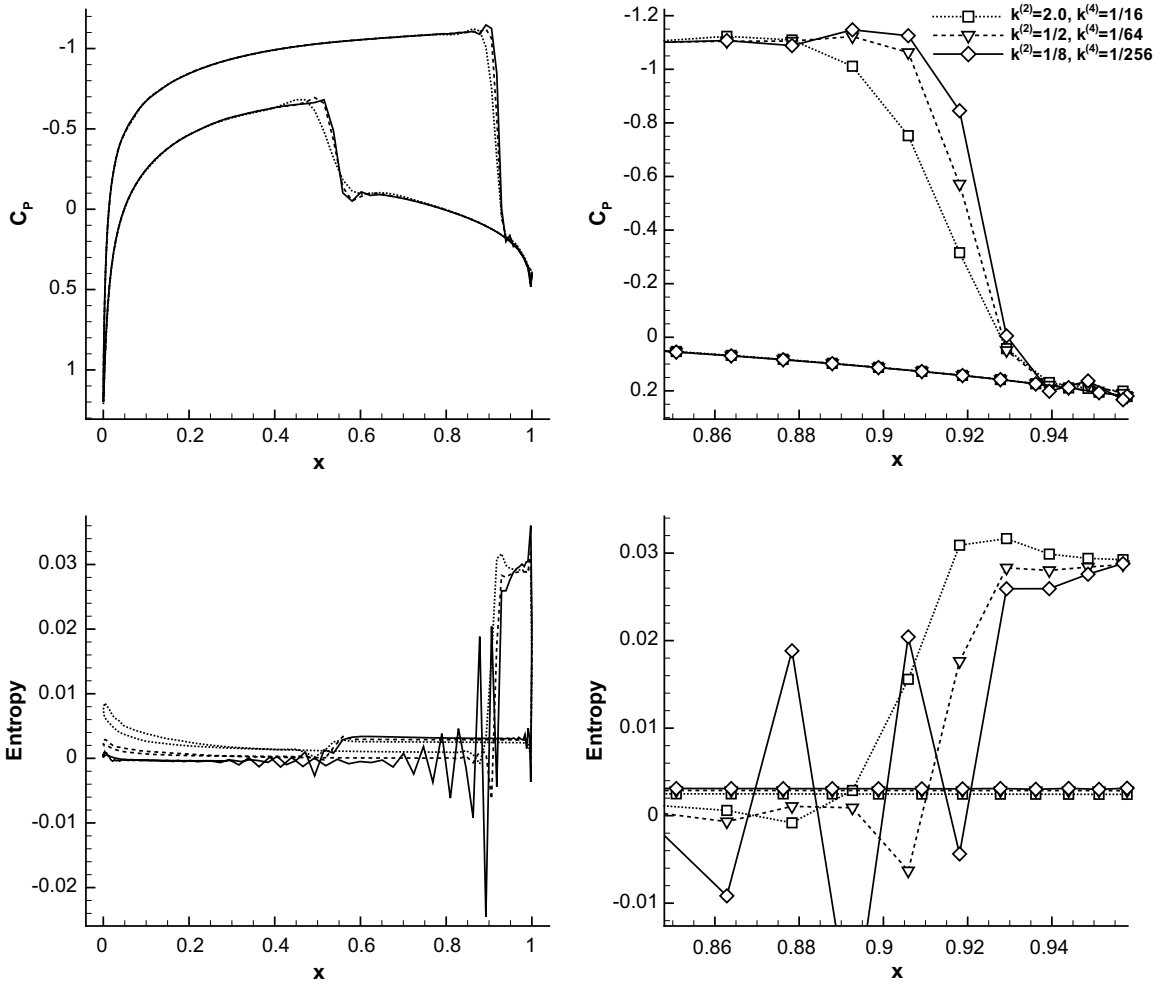

Fig. 2. Surface pressure coefficient and entropy for an inviscid transonic NACA0012 on the coarsest grid for a sequence of dissipation levels. The right-hand plots show a zoom of the main shock.

following: $C_D = 0.0$, and $C_L = 0.0$ by symmetry. The farfield is at a distance of 100 chord lengths in order to keep errors due to the finite domain small. The JST scheme is applied, and since the solution is smooth everywhere the shock switch (4) is $\mathcal{O}(h^2)$ and the added dissipation terms are $\mathcal{O}(h^3)$. A sequence of three hierarchically and globally refined triangular grids are considered. Grid 0 has ~5500 nodes, grid 1 ~22,000 nodes, and grid 2 ~88,000 nodes.

Despite the absence of shocks small oscillations in the solution exist, and when a sequence of calculations is performed with progressively reduced values of $k^{(2)}$ and $k^{(4)}$ these oscillations grow, emanating from the stagnation point and trailing edge. In contrast consider the effect on the drag of $k^{(4)}$ reduction, plotted in Fig. 3 twice, once on a linear scale, and once on a logarithmic scale. Here the points represent calculations on one of the three grids with various dissipation coefficients; with $k^{(2)} = \frac{1}{2}$, $k^{(4)}$ is repeatedly halved until the computation exhibits strong oscillations. Due to the absence of shocks it is also reasonable to set $k^{(2)} = 0$ and perform the same procedure.

It is apparent from the graphic that repeatedly halving dissipation causes the drag to appear to converge roughly linearly to an asymptote at $k^{(4)} = 0$. In fact this asymptote does not exist: the method becomes unstable before it is reached. Nonetheless the apparent limiting values may be estimated using Richardson extrapolation, and these are plotted as horizontal lines on the right-hand plot of Fig. 3. A schematic model of the sources of error involved has already been presented graphically in Fig. 1 where oscillation error, dissipation

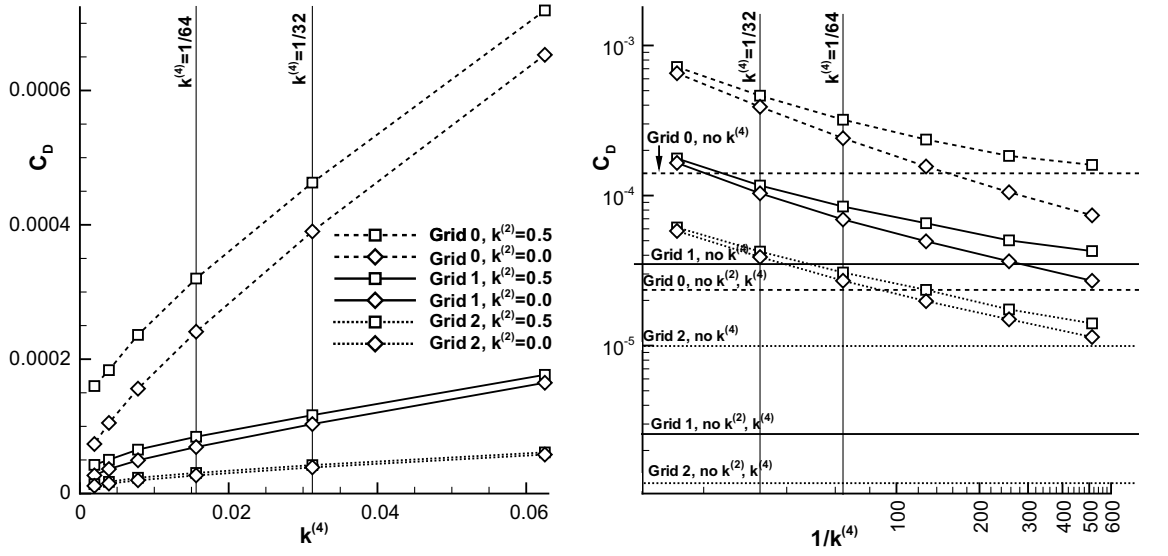

Fig. 3. Effect of dissipation reduction on drag for a subsonic NACA0012 case on a sequence of three globally refined grids. The right-hand plot uses a logarithmic scale for C_D.

smoothing error, and the remaining discretization error are distinguished. Here all errors are shown as additive, but in general they may also cancel.

Extrapolation is therefore valid if the drag error is taken to consist of the two distinct components already mentioned: oscillation error and smoothing error. If the latter corresponds to the effect of ϵ in the continuous Eq. (6), then a limit of zero dissipation is reasonable. The extrapolation will then be accurate if, in the region from which it is performed, the oscillation error is negligible – for example from the circle marked in Fig. 1.

Drag and lift are more suitable for such extrapolation than the solution itself because they exhibit apparent convergence for much lower values of $k^{(2)}$ and $k^{(4)}$. This is a consequence of forces being weighted sums of surface pressure over the aerofoil. Oscillatory errors then tend to cancel, especially as they are often distinguished by a regular odd–even decoupling of the solution at neighbouring mesh points, an example of which was seen in Fig. 2.

The extrapolated value allows an approximation to that proportion of the error in drag due to the smoothing effects of dissipation to be made. Let J^0 be the exact value of the cost function, $J^{(4)}$ the extrapolated value as $k^{(4)} \to 0$, and J^D the extrapolated value as $k^{(2)}$ and $k^{(4)}$ simultaneously approach zero ($k^{(2)} \to 0$) alone is not considered as decreasing second-, *increases* fourth-dissipation by (3). The total error in a cost function evaluation J is

$$\delta^0 = J - J^0,$$

while the total dissipation error and $k^{(4)}$ error are defined as

$$\delta^D = J - J^D, \quad \delta^{(4)} = J - J^{(4)},$$

respectively. Further the complement of $\delta^{(4)}$ in the total dissipation error is defined by

$$\delta^{(2)} = \delta^D - \delta^{(4)}.$$

Of particular interest are the proportions of δ^0 to the three dissipation error terms.

These values for the three cases of Fig. 3 are given in Table 1, where J is evaluated with $k^{(2)} = 1/2$ and both $k^{(4)} = 1/32$ and $1/64$. Firstly, note that the proportions of error due to each type of dissipation are similar for all three grids, testifying to the reliability of the extrapolation. The fourth-derivative dissipation terms dominate somewhat, as might be expected in a subsonic flow. More surprising is that the dissipation as a whole completely dominates the total error, accounting for more than 90% in all cases. One particularly striking manifestation of this result, which is most clearly visible in Fig. 3, is that by eliminating the effect of dissipation

Table 1
Error breakdown of drag for subsonic NACA0012 on three grids obtained by uniform refinement, including proportion of the total error due to dissipation

Grid	$k^{(4)}$	δ^0 ($\times 10^{-4}$)	δ^D ($\times 10^{-4}$)	% $\delta^{(2)}/\delta^0$	% $\delta^{(4)}/\delta^0$	% δ^D/δ^0
0	32	3.20	3.04	25	70	95
	64	4.63	4.31	37	56	93
1	32	0.845	0.828	28	70	98
	64	1.17	1.13	38	59	97
2	32	0.307	0.298	21	77	97
	64	0.423	0.415	28	68	98

from C_D evaluated on grid 0, we obtain a reduction in the error of a factor of more than 10, roughly equivalent to the increase in accuracy obtained by globally refining the grid twice.

One unusual feature of the second-order JST scheme is that for smooth solutions the dissipation terms are both of order h^3, while the error due to the central difference of the flux is h^2. Therefore, in the limit $h \to 0$ the error due to the dissipation must become of secondary importance, though this is not yet visible on the grids considered. The questions arise: at what level of grid resolution (and corresponding level of error) does this occur, and is this in the range of engineering interest? An accuracy level of practical interest for cases such as this was recently defined by representatives of the aerospace industry within the European project *ADIGMA* (which is concerned with the efficiency of higher-order accurate methods [33]) as ± 5 drag counts ($\pm 5 \times 10^{-4}$) and $\pm 1/2$ lift counts ($\pm 5 \times 10^{-3}$). Even if we conservatively demand 10 times that accuracy, grid 2 for the subsonic NACA0012 case (with default dissipation coefficients) is sufficient, and for that grid the dissipation contributes all but 1/20th of the error. Hence it is reasonable to expect that for engineering grid resolutions dissipation will be the dominant source of error for JST.

It should be noted that there are several schemes that are considered to be superior in accuracy to JST while comparable in cost, e.g. central schemes with matrix dissipation coefficients [27], CUSP [34,35] and AUSM-DV [30]. It is to be expected that if a similar analysis were performed on these schemes, the results corresponding to Table 1 would show a somewhat lesser influence of dissipation, negatively affecting the usefulness of a dissipation error estimator. However – without having investigated this issue numerically – the overwhelming dominance of dissipation error seen in the above computations suggests that dissipation will play a very significant role for these improved fluxes also.

4.2. Dissipation study: transonic ONERA M6 wing

As a more challenging example a three-dimensional transonic case, the ONERA M6 wing at $\alpha = 3.06$, and $M_\infty = 0.84$ is considered. Surface pressure contours are shown in Fig. 4 where the characteristic lambda shock structure is visible. Since the surface mesh consists of unstructured triangles there is no opportunity for numerical instability to manifest itself as clean odd–even decoupling as was the case in two-dimensions, though oscillations do occur. Nevertheless Fig. 4 shows clean convergence of C_D as the dissipation is reduced, with zero dissipation asymptotes in close agreement with a reference solution on grid 3, which has $\sim 55 \times 10^6$ nodes (grid 0 has $\sim 110 \times 10^3$ nodes, globally refined grid 1 has $\sim 820 \times 10^3$ nodes).

As before an error breakdown is computed based on the extrapolated coefficients, Table 2, whereby the convincing domination of the dissipation error is once again evident, although this time the second-derivate contributes the largest error as might have been anticipated in this shock-heavy flow. Another difference is the cancellation of error between the two forms of dissipation on grid 0, and between dissipation and other parts of discretization error on grids 0 and 1. Nevertheless the convergence of drag with dissipation reduction is again roughly linear, as can be better seen in Fig. 6 of the following section.

The effect of varying dissipation on the surface pressure is correspondingly dramatic. Pressure and entropy from a streamwise cut through the wing are plotted in Fig. 5 for a variety of dissipation levels on grid 0, and a single reference solution on grid 3. Apparent is the very significant improvement in shock sharpness and suction peak height achieved as dissipation is reduced.

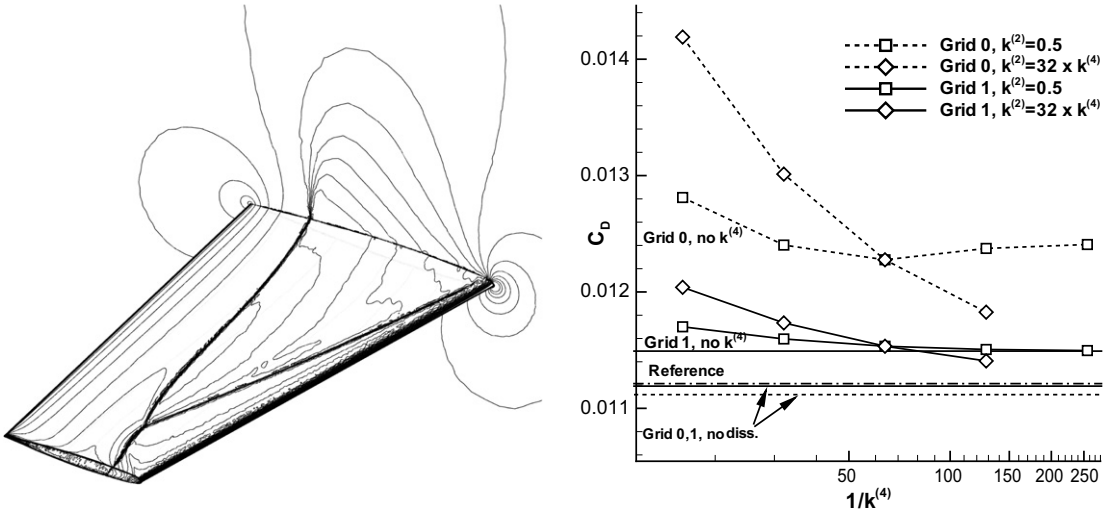

Fig. 4. Transonic ONERA M6 wing with lambda shock structure (left), and the effect of dissipation reduction on C_D for a coarse and once globally refined grid (right).

Table 2
Dissipation/total drag error breakdown for the transonic ONERA M6 wing

Grid	$k^{(4)}$	δ^0 ($\times 10^{-4}$)	δ^D ($\times 10^{-4}$)	% $\delta^{(2)}/\delta^0$	% $\delta^{(4)}/\delta^0$	% δ^D/δ^0
0	32	11.9	12.9	108	−0.4	108
	64	10.6	11.6	121	−12	109
1	32	3.84	4.03	78	27	105
	64	3.21	3.44	94	13	107

Reference $C_D = 0.011212$.

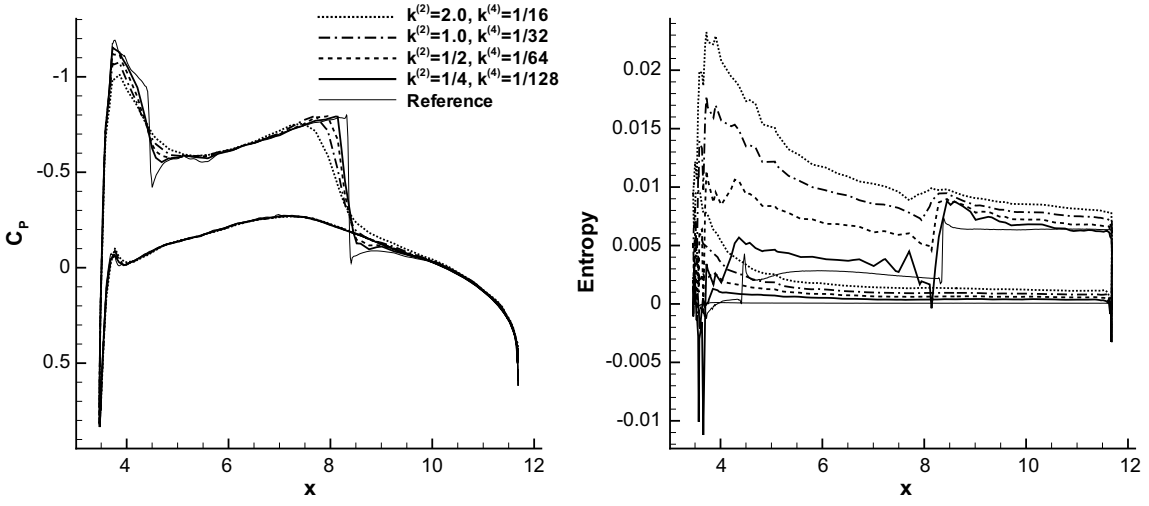

Fig. 5. Surface pressure coefficient and entropy for a cut at $y = 6$ through the ONERA M6 wing on a coarse grid for a sequence of dissipation levels. Reference solution on a thrice globally refined grid.

5. Application to goal-oriented adaptation

It is our intent to exploit the observations of the previous section for the purposes of improving solution accuracy. The most immediate approach might be to simply apply the extrapolation used above, and correct (several) goal functions with the error thereby identified, or possibly correct the entire solution. Because the dissipation error is a large and roughly constant proportion of the total error, we might expect a significant improvement in absolute accuracy, although no increase in order of grid convergence. A prime example is the subsonic NACA0012 of the previous section, in which an error reduction in drag equivalent to solution on twice globally refined grids was obtained.

However, such a method is likely to prove unreliable in practice. Richardson extrapolation is valid only in the limit of convergence, and this limit does not exist here because of the instability. Furthermore, such extrapolation is extremely sensitive to noise, and that is present in abundance due to spurious oscillations. These are likely to make correcting an entire solution even more problematic, although a means of eliminating this noise could make the approach tenable again – one possibility is post-processing with a Gibbs-complementary basis [36]. The choice of dissipation level sequence, and the necessity for at least three calculations with varying dissipation levels represent final hurdles.

A more robust alternative is to perform a local linearization about an initial solution, and then extrapolate linearly to a lower (or zero) level of dissipation. This is motivated by the approximately linear behaviour of the convergence seen in the cases of the previous section, and the observation that at least in the continuous case described by (6) the solution varies linearly with the level of added dissipation as $\epsilon \to 0$.

On this basis we propose a measure for the error in the JST scheme for a goal function J:

$$\eta = k^{(2)} \frac{\mathrm{d}J}{\mathrm{d}k^{(2)}} + k^{(4)} \frac{\mathrm{d}J}{\mathrm{d}k^{(4)}}, \tag{7}$$

whereby some means of evaluating the derivatives $\mathrm{d}J/\mathrm{d}k^{(2)}$ and $\mathrm{d}J/\mathrm{d}k^{(4)}$ is required.

The accuracy of η as an estimator of *dissipation* error relies on two opposing effects: (a) the linearity of the influence of added dissipation, which is satisfied in the low-dissipation limit, and (b) the small magnitude of oscillation error, which is satisfied in the large-dissipation limit. Any effective numerical flux may be expected to make a useful compromise between these two limits, and hence will be in a range where the estimator functions effectively. On the other hand the accuracy of η as an estimator of *total* discretization error depends on the extent to which dissipation error dominates other sources. As seen in the previous section – at least for integrated forces and the scheme considered – the former does dominate by a significant margin.

A mesh adaptation indicator for J may now be constructed by considering the influence of local variation of dissipation level. Let the dissipation coefficients be interpreted as being defined independently for each control volume,

$$\mathcal{K} = \left\{ k_i^{(2)}, k_i^{(4)} : \forall i \right\}$$

with the coefficient on a face being an average of immediate neighbours,

$$k_{ij}^{(2)} = \frac{1}{2}\left(k_i^{(2)} + k_j^{(2)}\right), \quad k_{ij}^{(4)} = \frac{1}{2}\left(k_i^{(4)} + k_j^{(4)}\right).$$

Now $\mathrm{d}J/\mathrm{d}k_i^{(2)}$ for example is a measure of the influence of the second-order dissipation in cell i on J, so an indicator for dissipation-error in J is

$$\xi_i = k^{(2)} \frac{\mathrm{d}J}{\mathrm{d}k_i^{(2)}} + k^{(4)} \frac{\mathrm{d}J}{\mathrm{d}k_i^{(4)}}. \tag{8}$$

The sensitivities of J with respect to all members of the parameter set $\mathcal{K}$ are required, and these may be efficiently and accurately evaluated using a discrete *adjoint* approach, which was developed for sensitivity evaluation in gradient based optimization. Implementation details are to be found in [37,23].

Consider the Lagrangian: $\mathcal{L}(w, \mathcal{K}, \psi) = J(w) + \psi^{\mathrm{T}} R(w, \mathcal{K})$, which always takes the value J provided the state equation $R(w, \mathcal{K}) = 0$ is fulfilled. Then for all $k \in \mathcal{K}$, $\mathrm{d}J/\mathrm{d}k = \mathrm{d}\mathcal{L}/\mathrm{d}k$, so that

$$\frac{\mathrm{d}J}{\mathrm{d}k} = \frac{\mathrm{d}\mathcal{L}}{\mathrm{d}k} = \frac{\partial J}{\partial w}\frac{\mathrm{d}w}{\mathrm{d}k} + \psi^{\mathrm{T}}\left\{\frac{\partial R}{\partial k} + \frac{\partial R}{\partial w}\frac{\mathrm{d}w}{\mathrm{d}k}\right\} \tag{9}$$

$$= \left\{\frac{\partial J}{\partial w} + \psi^{\mathrm{T}}\frac{\partial R}{\partial w}\right\}\frac{\mathrm{d}w}{\mathrm{d}k} + \psi^{\mathrm{T}}\frac{\partial R}{\partial k} = \psi^{\mathrm{T}}\frac{\partial R}{\partial k}, \tag{10}$$

whereby the final equality holds if ψ satisfies the *adjoint equation*

$$\frac{\partial R^{\mathrm{T}}}{\partial w}\psi = -\frac{\partial J^{\mathrm{T}}}{\partial w},$$

which is independent of the choice of variable $k \in \mathcal{K}$. For a given cost function ψ must therefore be evaluated only once in order to calculate the derivatives of J with respect to any number of parameters.

Given ψ the only additional computation expense in calculating ξ_i is the evaluation of $\partial R/\partial k$, which may be written down immediately. For $k_j^{(4)}$ for example it is

$$\frac{\partial R_i}{\partial k_j^{(4)}} = \begin{cases} \sum_{m\in\mathcal{N}(i)} -\frac{1}{4}|\lambda_{im}|\{L_m(w) - L_i(w)\} & j = i, \\ -\frac{1}{4}|\lambda_{ij}|\{L_j(w) - L_i(w)\} & j \in \mathcal{N}(i), \\ 0 & \text{otherwise} \end{cases} \tag{11}$$

and is always of the same order in h as the original dissipation term, so that away from singularities in the adjoint solution (which occur at sharp trailing edges in 2d transonic flows) the error indicator approaches zero as the mesh is refined. Treating the second- and fourth-derivative dissipation separately is not necessary, but the individual sensors offer additional insight into the behaviour of the JST scheme. Future work may consist in attempts to modify JST based on this analysis.

Note that the relations

$$\sum_i \frac{\partial R_i}{\partial k_j^{(4)}} = 0, \quad \sum_j \frac{\partial R_i}{\partial k_j^{(4)}} = \frac{\partial R_i}{\partial k^{(4)}},$$

hold, so that in particular

$$\eta = \sum_i \xi_i \tag{12}$$

and the sum of all local error indicators is the total error estimator as expected.

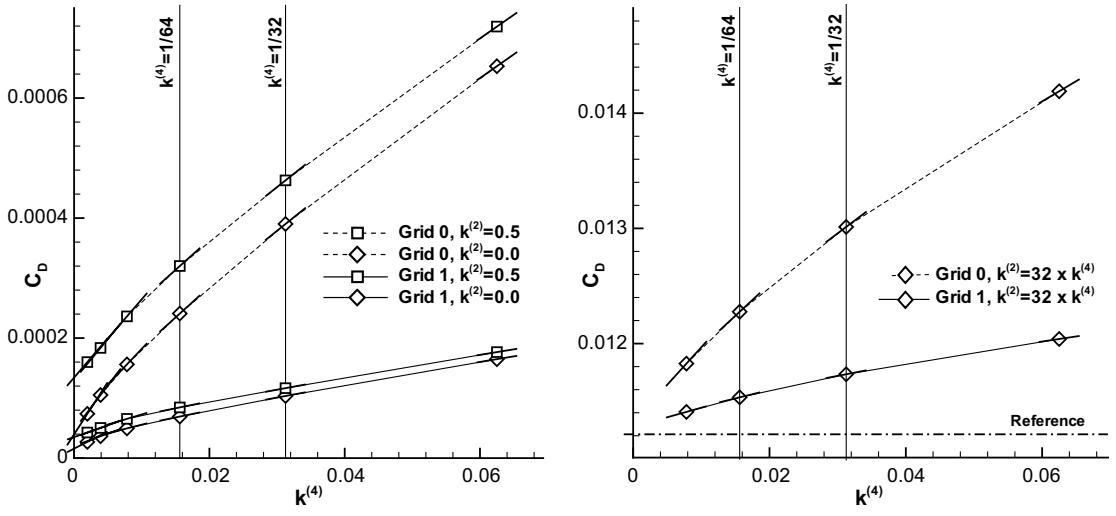

Fig. 6. Verification of gradients with respect to $k^{(2)}$, $k^{(4)}$ obtained with adjoint against the results of Section 4, for subsonic NACA0012 (left) and ONERA M6 (right).

The error measure for dissipation is closely related to existing error estimators such those of Ohlberger et al. [38–40], who devise an estimate of solution error in the L^1-norm which contains a local dissipation contribution of the more general form

$$Q_{ij}(w_i, w_j) := \frac{2\hat{f}_{ij}(w_i, w_j) - \hat{f}_{ij}(w_i, w_i) - \hat{f}_{ij}(w_j, w_j)}{w_i - w_j},$$

see e.g. [39]. If $\hat{f}$ is the JST scheme with $k^{(4)} = 0$, then Q_{ij} is exactly the coefficient of dissipation across the face $\{ij\}$. But $k^{(2)}\mathrm{d}J/\mathrm{d}k^{(2)} = k^{(2)}\psi^{\mathrm{T}}\partial R/\partial k^{(2)}$ is also the coefficient of dissipation – in this case multiplied by the adjoint solution because we are examining the influence on a target functional. Detailed examination of the relationship of these estimators will be the subject of further work.

The correctness of the implementation may be verified by plotting the calculated gradients of J with respect to $k^{(2)}$ and $k^{(4)}$ on the convergence graphs of the previous section. Fig. 6 reproduces the results of Figs. 3 and 4, with the gradients calculated by adjoint as short bars centered on the calculated points.

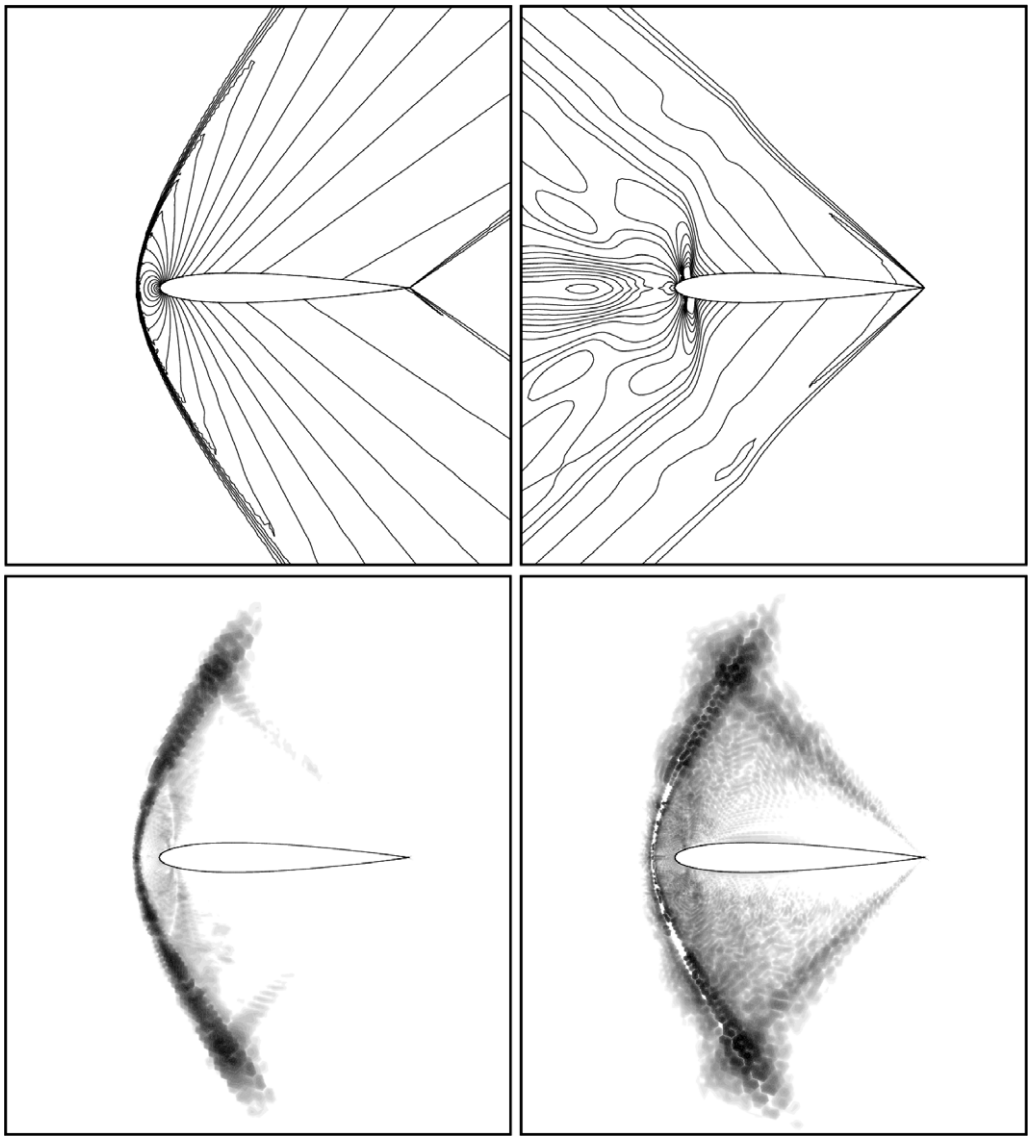

Fig. 7. Error indicator contours for supersonic NACA0012 drag: pressure (top left), first adjoint variable (top right), $k^{(2)}$, $k^{(4)}$ sensitivity (bottom left, right, respectively). The two sensor plots use the same (logarithmic) scale, where dark regions represent large indicator values.

The error indicator is briefly examined for an inviscid supersonic NACA0012 case with $M_\infty = 1.5$ and $\alpha = 1.0$, for which contours of pressure are shown in Fig. 7. The flow is supersonic everywhere expect for a small region around the stagnation point; as a result information transport is to a large extent unidirectional and errors produced downstream of the aerofoil do not influence lift or drag. This behaviour is captured by the adjoint solution (also shown), and is conferred on ξ. The two terms of the indicator in (8) are also plotted in Fig. 7, where the relative influence and regional activation of the two dissipation terms – $k^{(2)}$ active near the shock, and $k^{(4)}$ partly switched off there – as well as the effect of the adjoint solution are visible.

The irregularity of the indicator, which is partly due to its necessarily high sensitivity to the grid, demands that a small amount of smoothing is applied. Here and in the following, two Laplacian smoothing passes with a coefficient of 0.5 are used. All else being equal, a smooth mesh is likely to give a higher absolute accuracy than an irregular mesh, as the finite volume method described is quite sensitive to rapid variations in cell size and irregular cells. However, the indicator also has the effect of damping existing irregularities in the mesh by identifying regions of low resolution within regions of high resolution and adapting them preferentially. The quality of the meshes has therefore not been seen to deteriorate significantly in the course of multiple adaptation cycles, and the eventual convergence of the iteration is not affected.

6. Numerical results

To quantify the effectiveness of the error indicator and estimator we consider three inviscid NACA0012 aerofoil test-cases: the subsonic, transonic (considered in a similar context by Barth [10]) and supersonic cases already described. The default levels of second- and fourth-order artificial dissipation are taken, and for each case we consider both lift and drag adaptation.

We proceed as follows: on an initial mesh a flow solution is computed, followed by an adjoint solution for J, based on which the indicator and estimator are evaluated. The mesh is refined, whereby the percentage of new points introduced is fixed at 40% in 2d and 80% in 3d, and a new flow solution is computed, etc. All components of this chain are parallelized and no stopping criteria is used, rather the calculation halts when available computing resources are exhausted.

The mesh is adapted according to an indicator value which is assigned to each edge of the mesh. A threshold value is calculated such that the required percentage of new points is approximately achieved, and the corresponding edges are marked for refinement. For example in 2d, triangles with one edge marked are split into two with a new edge connecting the midpoint of the marked edge with the opposing vertex, and triangles with all edges marked are divided into four similar triangles. If only two edges of a triangle are marked the third is also marked, causing refinement in a neighbouring triangle. Mesh coarsening is not allowed.

For the subsonic case the analytic force coefficients are known. To obtain reliable and accurate estimates in the other cases an initial coarse mesh of 11×10^3 points is refined globally five times, resulting in a mesh of about 11×10^6 million points. Where points are added on the aerofoil's surface, their position is reconstructed using cubic splines. A flow computation is performed on each of these meshes, and Richardson extrapolation (on h this time) is applied to the three finest results to estimate the limiting value. This result is used as a reference solution.

For the purposes of comparison a feature-based adaptation indicator is considered. The idea is that large errors are made locally where solution gradients are large with respect to the cell spacing. For some flow variable ϕ the indicator on a mesh edge $\{ij\}$ is [41]:

$$\xi_{ij}^{\mathrm{FB}} = \sum_{\phi} \omega_\phi h^q |\phi_j - \phi_i|, \tag{13}$$

where $q \geqslant 0$ adjusts the rate at which the indicator approaches zero as the mesh is refined, and ω_ϕ are constant flow variable weights. In the following $q = 0$ and the variables total pressure and total enthalpy are used with equal weighting.

The mesh convergence for all cases and methods discussed so far is displayed in Fig. 8 where errors are calculated with respect to the reference solutions. For the error indicator results the error estimate (12) and the therewith corrected coefficient values are also plotted. Immediately evident is that the feature-based indi-

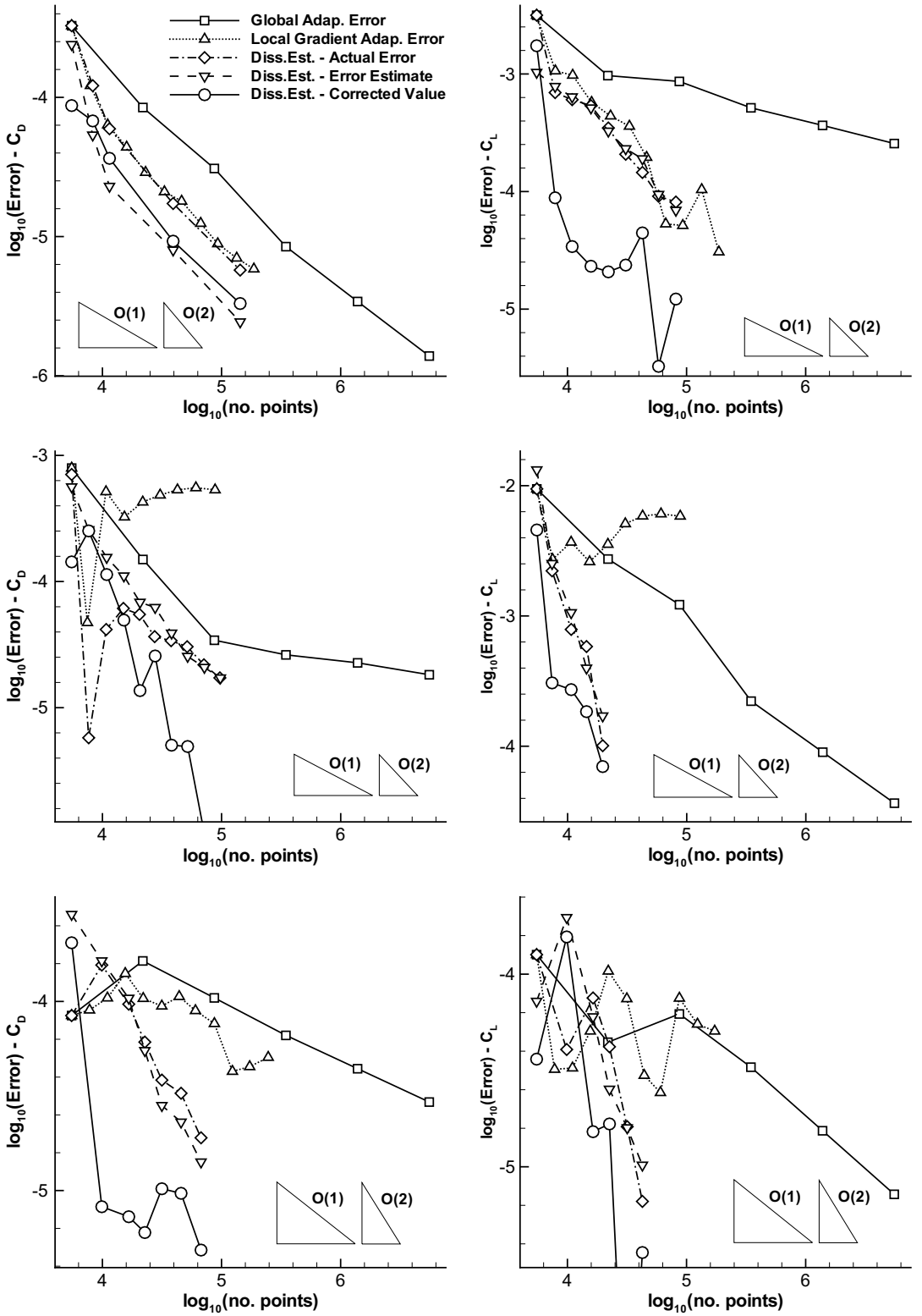

Fig. 8. Convergence of C_D (left) and C_L (right) errors for global, local-gradient and dissipation-error refinement, for sub-, trans- and supersonic cases (top to bottom). Error estimator and corrected error are shown for the proposed indicator.

cator only converges in the subsonic case, where the problem has an elliptic nature – in the transonic case it even converges to an incorrect value. Variation in choice of ϕ, q and percentage of new points has no effect on the character of these results. The poor suitability of standard feature-based indicators for trans- and supersonic flows is well known, but these findings emphasize the pressing need for a cheap and reliable alternative.

The dissipation-error adaptation performs consistently well. In the subsonic cases it matches the accuracy of feature-based refinement. In all other cases, if the greatest accuracy achieved by global refinement is regarded, the same error is achieved by error indicator refinement with roughly a factor of 100 fewer points. Taking into account the expense of the necessary adjoint computation, which is approximately as costly as the corresponding flow solution, the error indicator method is about 50 times more efficient than global refinement. In addition to this the error estimates are a good approximation of the actual error in all cases, and the corrected values are as a consequence consistently more accurate then the uncorrected values.

The corresponding meshes produced by the two indicators are shown in Fig. 9, and have been chosen to have similar numbers of points. The feature-based meshes are notable for their smoothness, regularity, and sharp resolution of shocks, but note that in the supersonic case many points are wasted resolving the fish-tail shock structure, which can not influence the surface pressure, as already noted. The error indicator meshes are irregular, but capture the information transport properties of the flow. Finite volume schemes are typically sensitive to non-smooth meshes, and so the good error reduction results of the indicator come *despite* its irregular nature. It is therefore anticipated that additional accuracy may be won by using more sophisticated indicator smoothing.

Given its success the error indicator may be applied to find out where the feature-based indicator is going wrong. The error indicator evaluated on a five-times feature-based adapted mesh is shown in Fig. 10. At each adaptation step the two shocks were refined, producing exceptionally high resolution there and much lower resolution in immediately neighbouring regions. The $k^{(2)}$ component of the error indicator is hence small everywhere, and the indicator structures seen in Fig. 10 are almost entirely from due to the $k^{(4)}$ component. The error indicator would favour a broadening of resolution about the shocks and fewer points inside the shock, suggesting that the shock position may be in error.

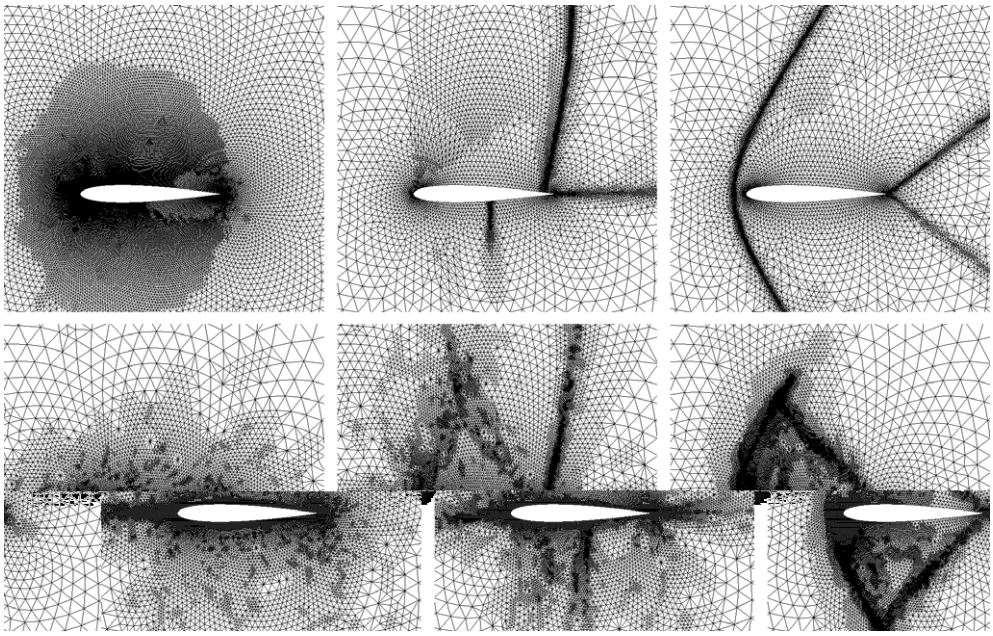

Fig. 9. Meshes for sub-, trans- and supersonic cases using solution gradient adaptation (top), and dissipation-error adaptation for C_L (bottom). All grids have a similar number of points.

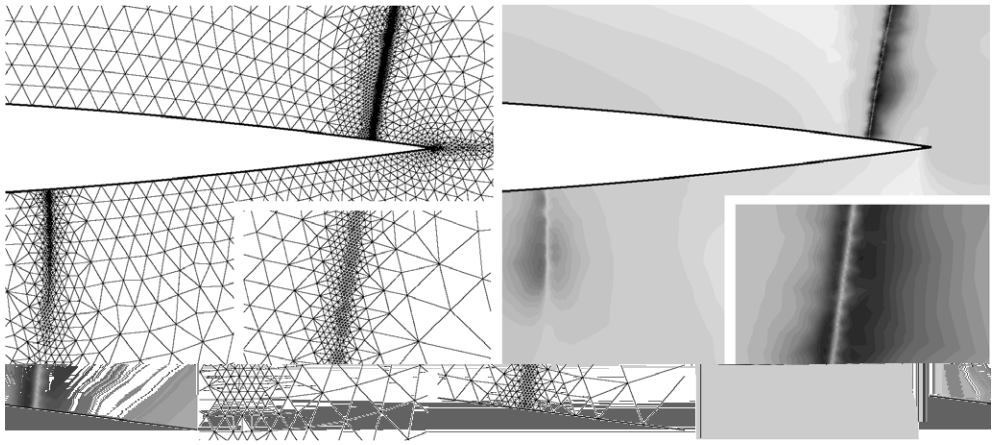

Fig. 10. Dissipation-based error indicator on mesh refined using feature-based adaptation. Dark regions represent large indicator values.

6.1. Adaptation of ONERA M6 Wing

Finally the method is applied in 3d to the ONERA M6 transonic test-case described in Section (4). A new difficulty encountered in three-dimensions was the robust and smooth reconstruction of the surface of the wing. The mesh adaptation routines do not at present have the continuous CAD geometry definitions available to them, and so use a cubic-spline surface reconstruction on the basis of the initial input mesh. Such reconstruction is difficult to perform accurately and robustly in 3d; as a consequence the algorithm has several user tuneable parameters, effectively resulting in ambiguity in surface definition. On the basis of two calculations on a three-times refined mesh with $\sim 55 \times 10^6$ nodes with different reasonable reconstruction parameters, a variation of about 0.5 drag counts and 0.05 lift counts was observed. The former is smaller than the observed discretization error, but the latter is of the same order of magnitude. As a consequence in the following the reference lift is taken from the finest grid achieved with goal-oriented adaptation on lift. This value lies within bounds given by the two results on the globally refined mesh.

Convergence results are given in Fig. 11. Horizontal lines mark the engineering accuracy bounds of the ADIGMA project for drag, and one-tenth the bound for lift (all calculations satisfied the standard lift bound).

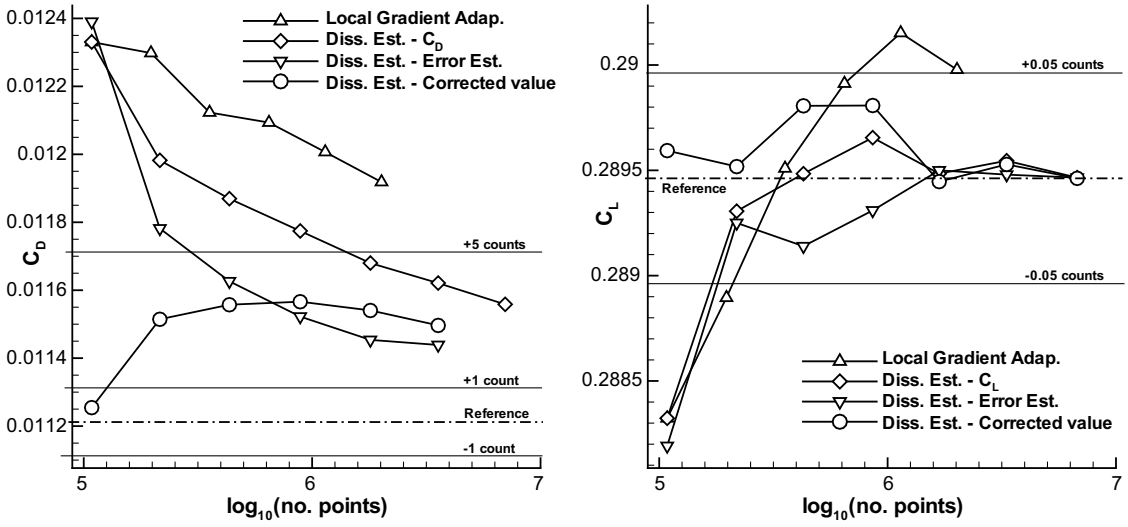

Fig. 11. Convergence of C_D (left) and C_L (right) for local-gradient and dissipation-error refinement for the ONERA M6 wing. Error estimator and corrected solution are also plotted.

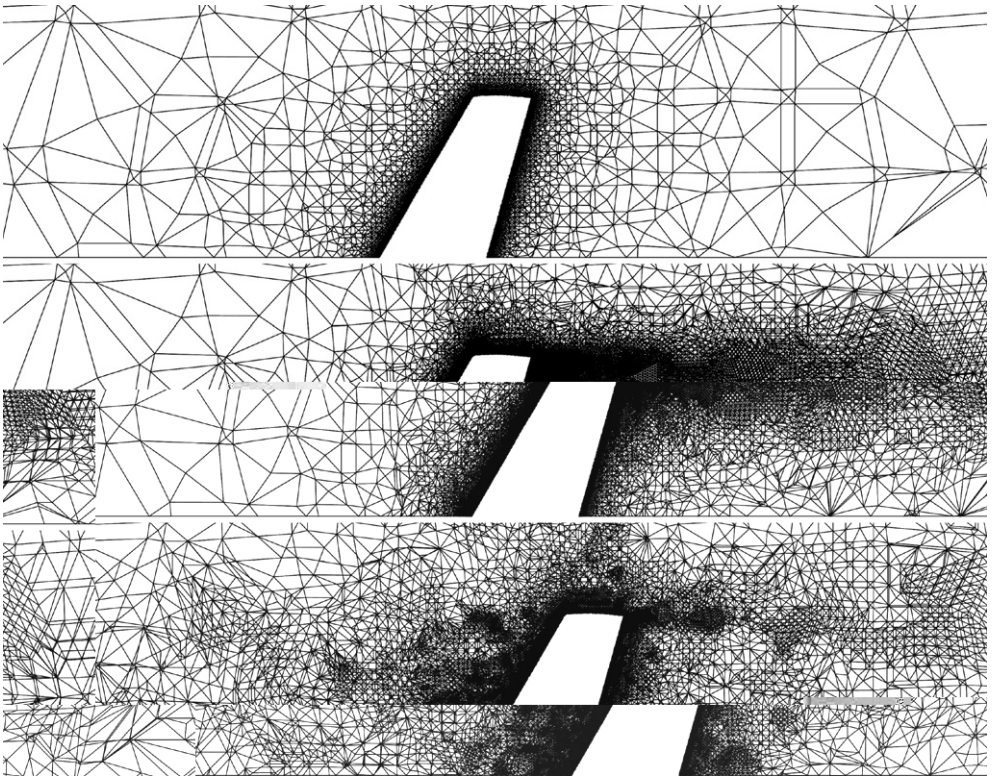

Fig. 12. ONERA M6 initial, local-gradient, and error indicator (drag) adapted grids cut at $y = 6$. The two adapted grids have a similar number of nodes.

As in 2d, feature-based adaptation performs poorly, and the error indicator significantly better, however particularly striking is that the corrected coefficient values all lie within the given accuracy bounds, even on the initial grid – in fact the estimator is most accurate on the initial grid. This may be a consequence of the error that is estimated, being the same as the error that is reduced by the adaptation. As the adaptation progresses that part of the error not due to dissipation will eventually dominate. Cuts through the grids obtained with the two adaptation methods are given in Fig. 12 where the relative irregularity of the grid based on the error indicator is once more evident.

7. Conclusions and further work

The connection between the level of added dissipation in an unstructured finite volume method based on a JST flux and the solution error, particularly in integrated force coefficients, has been investigated in an *a posteriori* manner. It has been seen that error due to the smoothing effect of dissipation accounts for at least 95% of the total error in drag for the two cases and five grids considered. Furthermore, this dissipation error varies almost linearly with the coefficients $k^{(2)}$ and $k^{(4)}$ of JST.

Using these observations a practical error estimator and corresponding goal-oriented mesh adaptation indicator have been proposed. Using the derivatives of a goal function with respect to locally defined dissipation coefficients a measure of the local influence of dissipation is obtained. The resulting method has an overhead of only a single adjoint solution per adaptation step, in contrast to existing techniques which require additionally a residual evaluation on a globally refined mesh. The scheme has been applied to both lift and drag estimation for a variety of cases in two- and three-dimensions, and functioned extremely accurately and consistently as both error indicator and total error estimator.

There are several avenues for further investigation. On the theoretical side the relationship to more general *a posteriori* error theories [4] demands investigation, as does the validity of the large dissipation error result for

other numerical fluxes and flow solvers. If a particular flux does not have a parameter controlling dissipation level (most upwind fluxes), one could be introduced taking a default value of unity, or other parameters such as Harten fix coefficients, or limiter settings could be examined. The influence of the initial mesh on convergence is an issue of great practical importance, especially given the lack of a mesh coarsening strategy. All initial meshes considered here are relatively fine, with increased resolution near regions of high surface curvature. If the adaptation strategy is comparably effective for very poor initial meshes substantial further cost savings in mesh generation could result.

From the practical point of view the most pressing issue is indicator non-smoothness which is likely to have an large effect on the results via the grid-sensitivity of the finite volume scheme. The challenge is to find a smoother which preserves major indicator features as well as the sum of the smoothed values (see (12). Error estimation for instationary problems will require some separate means of evaluating temporal discretization error, while the mechanics of mesh adaptation for moving domains has already been examined using gradient indicators [41].

The method is applicable to Navier–Stokes problems as it stands, given the availability of viscous adjoint solver and mesh refinement procedure for stretched quadrilateral and triangular cells. It is not anticipated that the discretization error of the viscous terms will be large, so dissipation error should still dominate, however whether or not the effect of dissipation will remain approximately linear is an open question.

References

[1] G. Warren, W. Anderson, J. Thomas, S. Krist, Grid convergence for adaptive methods, in: Proceedings of ICFD Conference on Numerical Methods for Fluids.
[2] C. Johnson, R. Rannacher, M. Boman, Numerics and hydrodynamics stability theory: towards error control in CFD, SIAM Journal of Numerical Analysis 32 (1995) 1058–1079.
[3] M. Giles, M. Larson, M. Levenstam, E. Süli, Adaptive error control for finite element approximations of the lift and drag coefficients in viscous flow, Tech. Rep. NA-97/06, Comlab, Oxford University, 1997.
[4] R. Becker, R. Rannacher, Weighted *a posteriori* error control in FE methods, in: Proceedings of ENUMATH-97, Heidelberg, World Scientific Publishing, Singapore, 1998.
[5] E. Süli, *A posteriori* error analysis and adaptivity for finite element approximations of hyperbolic problems, in: Kröner, Ohlberger, Rohde (Eds.), An Introduction to Recent Developments in Theory and Numerics for Conservation Laws, Lecture Notes in Computational Science and Engineering, vol. 5, Springer, Heidelberg, 1998, pp. 122–194.
[6] M. Giles, N. Pierce, Improved lift and drag estimates using adjoint Euler equations, in: American Institute of Aeronautics and Astronautics, Paper AIAA-1999-3293, 1999.
[7] S. Prudhomme, J. Oden, On goal-oriented error estimation for elliptic problems: application to the control of pointwise errors, Computer Methods in Applied Mechanics and Engineering (1999) 313–331.
[8] R. Hartmann, P. Houston, Adaptive discontinuous Galerkin methods for the compressible Euler equations, Journal of Computational Physics 182 (2) (2002) 508–532.
[9] T. Barth, H. Deconinck (Eds.), Error Estimation and Adaptive Discretization Methods in CFD, Lecture Notes in Computational Science and Engineering, vol. 25, Springer, 2002.
[10] T. Barth, A-posteriori error estimation and mesh adaptivity for finite volume and finite element methods, Springer Series Lecture Notes in Computational Science and Engineering 41.
[11] T. Gerhold, M. Galle, O. Friedrich, J. Evans, Calculation of complex 3D configurations employing the DLR TAU-Code, in: AIAA Paper Series, AIAA-1997-0167, 1997.
[12] R. Dwight, Efficiency improvements of RANS-based analysis and optimization using implicit and adjoint methods on unstructured grids, Ph.D. thesis, School of Mathematics, University of Manchester, 2006.
[13] A. Harten, Multiresolution algorithms for the numerical solution of hyperbolic conservation laws, Communications in Pure and Applied Mathematics 48 (1995) 1305–1342.
[14] B. Bihari, A. Harten, Multiresolution schemes for the numerical solution of 2-D conservation laws I, SIAM Journal of Scientific Computing 18 (2) (1997) 315–354.
[15] W. Dahmen, Wavelet and multiscale methods for operator equations, Acta Numerica 6 (1997) 55–228.
[16] S. Müller, Adaptive Multiscale Schemes for Conservation Laws, Lecture Notes in Computational Science and Engineering, vol. 27, Springer, Berlin, 2003, iSSN 1439-7358.
[17] D. Venditti, D. Darmofal, Anisotropic grid adaptation for functional outputs: application to two-dimensional viscous flows, Journal of Computational Physics 187 (2003) 22–46.
[18] N. Pierce, M. Giles, Adjoint and defect error bounding and correction for functional estimates, Journal of Computational Physics 200 (2004) 769–794.
[19] W. Jones, E. Nielsen, M. Park, Validation of 3d adjoint based error estimation and mesh adaptation for sonic boom prediction, in: 44th AIAA Aerospace Sciences Meeting and Exhibit, Reno, Nevada. Paper AIAA-2006-1150.

[20] M. Giles, M. Duta, J.-D. Muller, N. Pierce, Algorithm developments for discrete adjoint methods, AIAA Journal 41 (2) (2003) 198–205.
[21] E. Nielsen, M. Park, Using an adjoint approach to eliminate mesh sensitivities in aerodynamic design, AIAA Journal 44 (5) (2005) 948–953.
[22] D. Mavriplis, Multigrid solution of the discrete adjoint for optimization problems on unstructured meshes, AIAA Journal 44 (1) (2006) 42–50, Paper 0001-1452.
[23] R. Dwight, J. Brezillon, D. Vollmer, Efficient algorithms for solution of the adjoint compressible Navier–Stokes equations with applications, in: Proceedings of the ONERA-DLR Aero Symposium, 2006.
[24] M. Nemec, M. Aftosmis, Adjoint error estimation and adaptive refinement for embedded-boundary Cartesian meshes, in: 18th AIAA CFD Conference, Miami. Paper AIAA-2007-4187.
[25] R. Dwight, Goal-oriented mesh adaptation using a dissipation-based error indicator, in: Proceedings of ICFD Conference, University of Reading, 2007.
[26] A. Jameson, W. Schmidt, E. Turkel, Numerical solutions of the Euler equations by finite volume methods using Runge–Kutta time-stepping schemes, in: AIAA Paper Series, AIAA-1981-1259, 1981.
[27] E. Turkel, Improving the accuracy of central difference schemes, ICASE Report(88-53).
[28] B. Van Leer, Flux-vector splitting for the Euler equations, in: Proceedings of Eighth International Conference on Numerical Methods in Fluid Dynamics, Aachen, Springer-Verlag, 1982, pp. 507–512.
[29] P. Roe, Characteristic-based schemes for the Euler equations, Annual Review of Fluid Mechanics 18 (1986) 337–365.
[30] Y. Wada, M.-S. Liou, A flux splitting scheme with high-resolution and robustness for discontinuities, Collection of Papers on Aerospace Science (1994) 10–13.
[31] C.B. Laney, Computational Gasdynamics, Cambridge University Press, Cambridge, 1998.
[32] A. Brooks, T. Hughes, Streamline upwind/Petrov–Galerkin formulations for convection dominated flows with particular emphasis on the incompressible Navier–Stokes equations, Computer Methods in Applied Mechanics and Engineering (1990) 199–259.
[33] N. Kroll, ADIGMA – A European project on the development of adaptive higher order variational methods for aerospace applications, in: Proceedings of ECCOMAS, Egmond aan Zee, 2006.
[34] A. Jameson, Analysis and design of numerical schemes for gas dynamics I: artificial diffusion, upwind biasing, limiters and their effect on accuracy and multigrid convergence, International Journal of Computational Fluid Dynamics 4 (3–4) (1995) 171–218.
[35] A. Jameson, Analysis and design of numerical schemes for gas dynamics II: artificial diffusion and discrete shock structure, International Journal of Computational Fluid Dynamics 5 (1) (1995) 1–38.
[36] G. May, A. Jameson, High-order accurate methods for high-speed flow, in: AIAA Paper Series, Paper 2005-5251, AIAA, 2005.
[37] R. Dwight, J. Brezillon, Effect of approximations of the discrete adjoint on gradient-based optimization, AIAA Journal 44 (12) (2006) 3022–3071.
[38] D. Kröner, M. Ohlberger, *A posteriori* error estimates for upwind finite volume schemes for nonlinear conservation laws in multi dimensions, Mathematics of Computation 69 (2000) 25–39.
[39] M. Ohlberger, *A posteriori* error estimates for vertex centered finite volume approximations of convection–diffusion–reaction equations, M2AN Mathematical Modeling and Numerical Analysis 35 (2001) 355–387.
[40] A. Dedner, C. Makridakis, M. Ohlberger, Error control for a class of Runge–Kutta discontinuous Galerkin methods for nonlinear conservation laws, SIAM Journal of Numerical Analysis 45 (2) (2007) 514–538.
[41] T. Alrutz, M. Rütten, Investigation of vortex breakdown over a pitching delta wing applying the DLR TAU-Code with full, automatic grid adaptation, Paper 5162, AIAA, 2005.